Molecular and electronic structures of copper-cuprizone and analogues

Suman Kundu,[a] Amiya Mondal,[a] Thomas Weyhermüller,[b] Stephen Sproules[c] and Prasanta Ghosh[a]*

[a]Department of Chemistry, R. K. Mission Residential College, Narendrapur, Kolkata 700103, India. Fax: +91-33 2477 3597; Tel: +91-33 2428 7347; E-mail: ghosh@pghosh.in

[b]Max-Planck-Institut für ChemischeEnergiekonversion, Stiftstrasse 34-36 / D-45470 Mülheiman der Ruhr, Germany.

[c]WestCHEM, School of Chemistry, University of Glasgow, Glasgow G12 8QQ, United Kingdom.

*Corresponding author. E-mail: ghosh@pghosh.in; Fax: +91 33 2477 3597; Tel: +91 33 2428 7347

Abstract

A paramagnetic dinuclear copper(II) complex, $[Cu^{II}(L^{-})Cl]_2$ (**1**) while LH = (*E*)-1,2-diphenyl-2-(2-(pyridine-2-yl)hydrozono)ethanone, an analogue of mono-hydrazone cuprizone ($L_{mcpz}H_2$), was isolated and substantiated by spectra, single crystal X-ray structure determination, unrestricted density functional theory (DFT) calculations and inter alia. Magnetic susceptibility measurement and EPR spectra confirmed the triplet state of **1** above 30 K because of two paramagnetic copper(II) centers. Unrestricted DFT calculations on copper cuprizone species with doublet spin state established similar electronic features and disclosed that bis-deprotonated NN-chelation, $[Cu(L_{mcpz})_2]^{2-}$, (*cis* or *trans*-$\mathbf{2}^{\mathbf{NN}}$), is ~3×10^3 kJ/mole higher in energy than the mono-deprotonated NO-chelation, $Cu(L_{mcpz}H)_2$, (*cis* or *trans*-$\mathbf{2}^{\mathbf{NO}}$) precluding the existence of so far reported $\mathbf{2}^{\mathbf{NN}}$ products. The calculations revealed that in all isomers, due to the mixing of $d_{x^2-y^2}$ orbital with a ligand group orbital as in **1**, 48-50% spin density is delocalized over the $L_{mcpz}H_2$ ligand. In fluid solution, **1** absorbs strongly at 527 nm due to LMCT elucidated by the time dependent (TD) DFT calculations and the excited LMCT state is fluorescent ($»_{ex}$ = 375 nm; $»_{em}$ = 405, 426 nm; ¦ = 0.014).

Keywords

Dinuclear copper(II) complex, copper cuprizone, electronic structure, DFT calculations

1. Introduction

Mono-hydrazone cuprizone ($L_{mcpz}H_2$) is a bioactive molecule with neurotoxic properties leading to spongiosis and is used as a drug to induce that in laboratory animals [1-7]. Cuprizone has a strong affinity towards the redox active copper ion but the origin of the bioactivity of it is not clear so far [8-10]. To analyze the electronic and structural features mimicking the copper cuprizone complex, copper parent osazone (PhNHN=CH-CH=NNHPh) complex was given attention. Reaction of osazone with copper(II) ion salt under argon in methanol affords a dark red precipitate which is unstable even in solid state and decomposes spontaneously at 298 K [11].

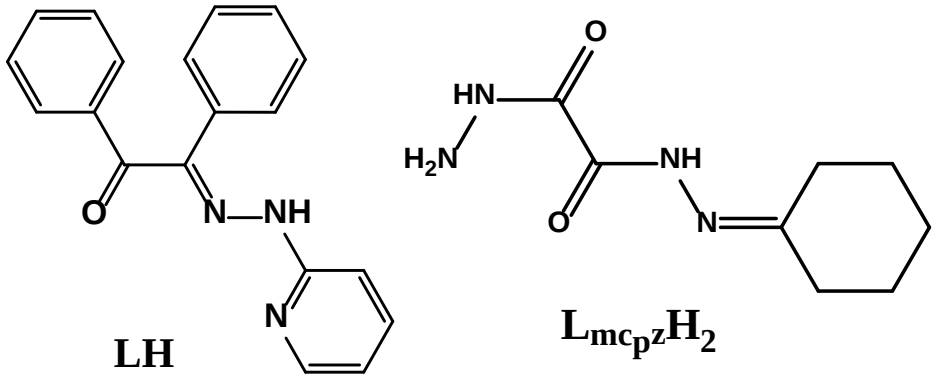

Chart 1 (*E*)-1,2-diphenyl-2-(2-(pyridine-2-yl)hydrozono)ethanone (LH) and mono-hydrazone cuprizone ($L_{mcpz}H_2$).

However, the reaction of benzil with 2-hydrazino pyridine in methanol in air yields a two electron paramagnetic dinuclear copper complex, $(CuLCl)_2$, **1,** of (*E*)-1,2-diphenyl-2-(2-(pyridine-2-yl)hydrozono)ethanone (LH), an analogue of mono-hydrazone cuprizone ($L_{mcpz}H_2$) as shown in Chart 1. A complete experimental and theoretical study substantiated the complex **1** which incorporates NNO chelate. To compare the ground state energies of the various chelation modes of cuprizone to copper(II) ion and the compositions of the molecular orbitals were analyzed by DFT calculations. The calculations on the paramagnetic $[Cu(L_{mcpz})]^{2-}$, ($\mathbf{2}^{NN}$) or $Cu(L_{mcpz}H)_2$, ($\mathbf{2}^{NO}$ or $\mathbf{2}^{OO}$) considering all three types of chelation as illustrated in Scheme 1, likewise, established that the frontier molecular orbitals of **1** are very similar to those of $\mathbf{2}^{NN}$, $\mathbf{2}^{NO}$ and $\mathbf{2}^{OO}$ analogues.

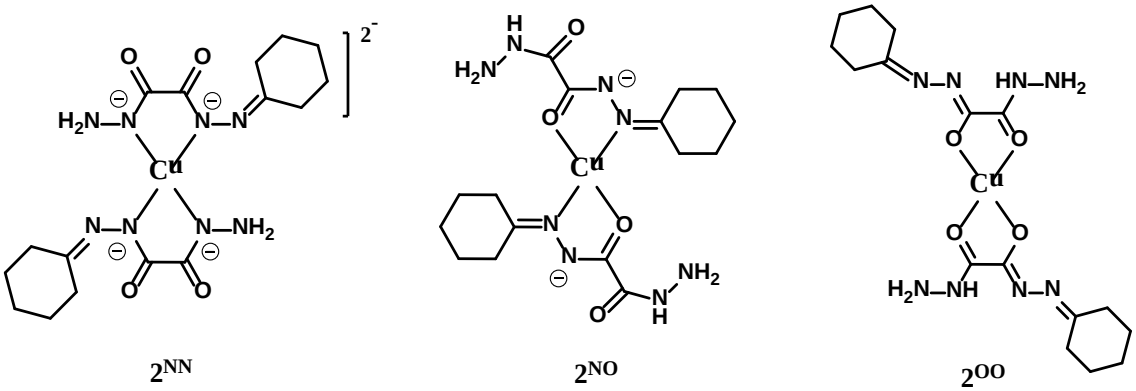

Scheme 1 Possible chelation modes of $L_{mcpz}H_2$: $[Cu(L_{mcpz})_2]^{2-}$ ($\mathbf{2}^{NN}$) and $[Cu(L_{mcpz}H)_2]$ ($\mathbf{2}^{NO}$ and $\mathbf{2}^{OO}$).

In this article, synthesis, structure, spectra and the unrestricted DFT calculations on **1**, *cis/trans* isomers of $\mathbf{2}^{\mathbf{NO}}$, $\mathbf{2}^{\mathbf{NN}}$ and $\mathbf{2}^{\mathbf{OO}}$ are reported.

2. Experimental

2.1. Materials and physical measurements

Reagents or analytical grade materials were obtained from *Sigma-Aldrich* and used without further purification. Spectroscopic grade solvents were used for spectroscopic measurements. After evaporating H_2O and MeOH solvents of the sample under high vacuum, elemental analyses and spectral measurements were performed. The C, H and N content of the compounds were obtained from *Perkin-Elmer 2400 series II* elemental analyzer. Infrared spectra of the samples were measured from 4000 to 400 cm^{-1} with the KBr pellet at 298 K on a *Perkin-Elmer Spectrum RX 1*, FT-IR Spectrophotometer. ESI mass spectra were recorded on a micro mass *Q-TOF mass spectrometer*. Electronic absorption spectra in solutions at 298 K were carried out on a *Perkin-Elmer Lambda 25* spectrophotometer in the range of 1100-200 nm. Variable temperature (3-300 K) magnetization data were recorded in a 1 T magnetic field on a *SQUID magnetometer* (MPMS Quantum Design). The experimental magnetic susceptibility data were corrected for underlying diamagnetism using tabulated Pascal's constants and fit using julX (Dr. Eckhard Bill). X-band EPR spectra were recorded on a Bruker ELEXSYS E500 spectrometer and simulated with XSophe [12] distributed by Bruker Biospin GmbH. The electro analytical instrument, *BASi Epsilon-EC* for cyclic voltammetric experiments in CH_2Cl_2 solutions containing 0.2 M tetrabutylammonium hexafluorophosphate as supporting electrolyte was used. The BASi platinum working electrode, platinum auxiliary electrode, Ag/AgCl reference electrode were used for the measurements.

2.2. Syntheses

2.2.1. $[CuLCl]_2$ (**1**)

To a mixture of benzil (105 mg, 0.5 mmol) and 2-hydrazino pyridine (55 mg, 0.5 mmol) in a 100 mL round bottom flask, methanol (50 mL) was added and the reaction mixture was refluxed for 45 min (338 K). After cooling at room temperature (298 K), the solution mixture was filtered. To this solution anhydrous $CuCl_2$ (70 mg, 0.5 mmol) in methanol (~10 mL) was added carefully and the

reaction mixture was allowed to evaporate slowly at 298 K. After a few days, a green crystalline solid of **1** separated out, which were filtered and dried in air and collected. Yield: 96 mg (~51% with respect to cupper). Mass spectrum (ESI, positive ion, CH_3CN); *m/z*: 363 for (CuL^+). Anal. Calc. for $C_{38}H_{28}Cl_2Cu_2N_6O_2$: C, 57.15; H, 3.53; N, 10.52; Found: C, 57.25; H, 3.55; N, 10.45. IR (KBr disk): ½3474 (s), 1602 (vs), 1456 (m), 1514 (m), 1466 (s), 1438 (s), 1358 (s), 1327 (s), 1208 (vs), 1141 (s), 1092 (s), 1012 (s), 927 (m), 778 (m), 702 (s), 665 (vs) cm^{-1}

2.3. Structure determination

Single crystals of **1** was picked up with nylon loops and was mounted on a *Bruker APEX-II CCD* diffractometer equipped with a Mo-target rotating-anode X-ray source and a graphite monochromator (Mo-K±, » = 0.71073 Å). Final cell constants were obtained from least squares fits of all measured reflections. Intensity data were corrected for absorption using intensities of redundant reflections. The structure was readily solved by direct methods and subsequent difference Fourier techniques. The crystallographic data of **1** are listed in Table 1. The Siemens SHELXS97 [13] software package was used for solution and SHELXL97 [13] was used for the refinement. All non-hydrogen atoms were refined anisotropically. Hydrogen atoms were placed at the calculated positions and refined as riding atoms with isotropic displacement parameters.

2.4. Density functional theory (DFT) calculations

All calculations reported in this chapter were done with the Gaussian 03W [14] programme package supported by GaussView 4.1. The DFT [15] and TD DFT [16] calculations were performed at the level of Becke three parameter hybrid functional with the non-local correlation functional of Lee-Yang-Parr (B3LYP) [17]. The gas phase geometries of **1**, ***t*-2NO**, ***c*-2NO**, ***t*-2^{NN}**, ***c*-2^{NN}** and **2^{OO}** were optimized on theoretical coordinates using Pulay's Direct Inversion [18] in the Iterative Subspace (DIIS) convergent SCF procedure [19] ignoring symmetry. In all calculations, a LANL2DZ basis set along with the corresponding effective core potential (ECP) was used for copper metal [20]. Valence double zeta basis set, 6-31G [21] for H was used. For C, N, O and Cl non-hydrogen atoms valence double zeta plus diffuse and polarization functions, 6-31G(d, p) [22] as basis set were employed for the calculations. The percentage contribution of ligand and metal to the frontier orbitals of **1** and ***t*-**

$\mathbf{2}^{NO}$ were calculated using GaussSum program package [23]. The sixty lowest singlet excitation energies on the optimized geometries of **1** in dichloromethane using CPCM model [24] were elucidated by TD DFT method.

Table 1 Crystallographic data for **1**.

CCDC	840632	ρ_c/g cm^{-3}	1.525
Formula	$C_{38}H_{28}Cl_2Cu_2N_6O_2$	2$_{max}$	50.0
F_w	798.64	Unique reflections	8375
Crystal colour	Green	Total reflections	12939
Crystal system	Monoclinic	»/Å	0.71073
Space group	*C2/c*	μ/mm^{-1}	1.421
a/Å	21.9360(5)	*F*(000)	1624
b/Å	9.8104(2)	R_1^a [*I*>2Ã(*I*)]	0.0257
c/Å	17.5925(4)	GOF^b	1.02
² /^{0}	113.27(1)	R_1^a (all data)	0.0297
V/Å^3	3477.87(13)	wR_2^c [*I*>2Ã(*I*)]	0.0743
Z	4	No. of Parameter	226
T/K	296(2)	• Á$_{max,min}$/eÅ^{-3}	0.508/-0.348

Observation criterion*: I > 2σ(I).* $^a R_1 = \Sigma||F_o|-|F_c||/\Sigma|F_o|$ ^{b}GOF = $\{\Sigma[w(F_o^2 - F_c^2)^2]/(n-p)\}^{1/2}$
$^c wR_2 = \{\Sigma[w(F_o^2-F_c^2)^2]/\Sigma[w(F_o^2)^2]\}^{1/2}$ where $w = 1/[\sigma^2(F_o^2) + (aP)^2+bP]$, $P = (F_o^2+2F_c^2)/3$

3. Results and discussion

3.1. Syntheses and characterization

The tridentate NNO-donor chelating agent, (*E*)-1, 2-diphenyl-2-(2-(pyridine-2-yl)hydrozno)ethanone (LH), was not pre-isolated. The reaction of benzyl and 2-hydrazinopyridine with anhydrous $CuCl_2$ in methanol affords **1** in a moderate yield (~51% with respect to copper). The composition of **1** was substantiated by mass, IR spectra and elemental analyses including the single crystal X-ray structure determination. Like copper-cuprizone complex with a lower energy absorption band at 609 nm, [8] **1** absorbs strongly at 527 nm. The electronic spectrum of **1** is shown in Fig. 1(a) and the spectral parameters are summarized in Table 2. TD DFT calculations elucidated the origins of such transitions (*vide infra*). The dichloromethane solution of **1** is fluorescent at 295 K. The structured excitation and emission spectra are illustrated in Fig. 1(b) and emission parameters are summarized in Table 2. The quantum yield was calculated with respect to anthracene.

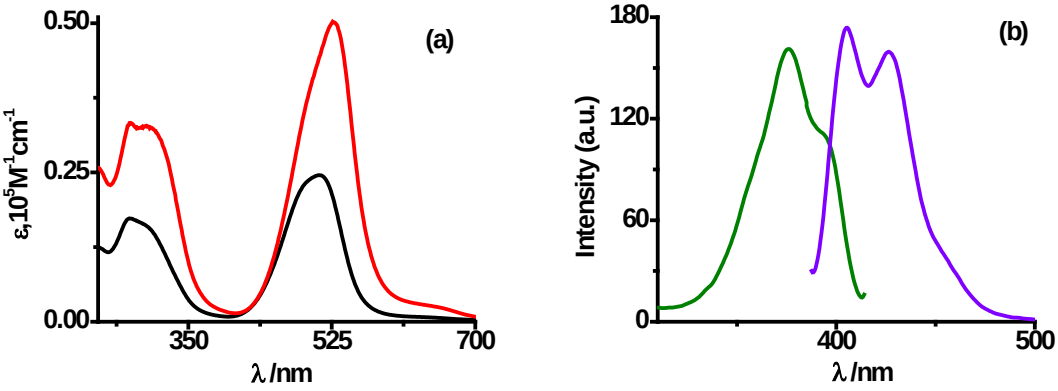

Fig. 1 (a) Electronic spectra in CH_2Cl_2 (red) and CH_3CN (black) and (b) excitation (green) and emission (violet) spectra in CH_2Cl_2 of **1** at 295 K.

Table 2 Electronic and fluorescence spectral data of **1** in CH_2Cl_2 and CH_3CN at 295 K.

Solvent	UV-vis spectral data $»_{max}$, nm (µ, 10^5 M^{-1} cm^{-1})	Fluorescence spectral data
CH_2Cl_2	527 (0.49), 301 (0.32), 280 (0.33)	$»_{ex}$ = 375 nm; $»_{em}$ = 405, 426 nm; ¦ = 0.014
CH_3CN	510 (0.25), 299 (0.16), 278 (0.17)	Non-emissive

3.2. X-ray structure of **1**

Single crystal X-ray structure determination confirmed the molecular geometry of **1** in crystals. It crystallizes in space group *C2/c*. The molecular structure with the atom numbering scheme is depicted in Fig. 2 and the relevant bond parameters are summarized in Table 3. In **1**, two $CuCl_2N_2O$ coordination spheres with distorted trigonal bipyramid (tbp) geometries are equivalent.

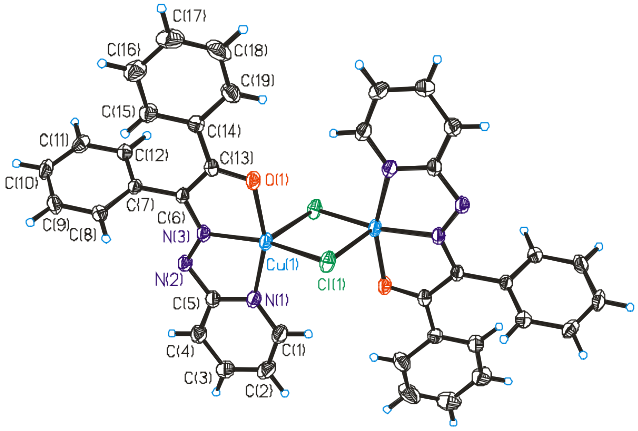

Fig. 2 Molecular structure of **1** in crystals.

Table 3 Selected experimental and calculated bond distances (Å) and angles (deg) of **1**.

	Experimental	Calculated
Cu(1)–N(1)	1.9896(17)	2.0491
Cu(1)–N(3)	1.9392(14)	2.0099
Cu(1)–O(1)	1.9922(14)	2.0342
Cu(1)–Cl(1)	2.2553(5)	2.3079
N(3)−N(2)	1.306(2)	1.2949
N(3)−C(6)	1.335(2)	1.3407
N(1)−C(5)	1.357(2)	1.3618
N(2)−C(5)	1.389(2)	1.3843
O(1)−C(13)	1.267(2)	1.2717
C(6)−C(13)	1.442(2)	1.4511
N(3)–Cu(1)–N(1)	79.07(6)	77.67
N(3)–Cu(1)–O(1)	80.34(6)	79.12
N(1)−Cu(1)−Cl(1)	100.20(5)	99.96
O(1)−Cu(1)−Cl(1)	97.37(4)	95.37
Cl(1)−Cu(1)−Cl(1)	92.921(18)	93.04

Cu(1), Cl(1), Cl(1A) and N(3) sites are on the equatorial plane with mean deviation 0.005 Å while O(1), Cu(1) and N(1) atoms make the axial bond with 158.91(6)°. The tridentate chelate with the pyridine ring is planar (mean deviation 0.04 Å). The orientations of the two pendant phenyl rings of the benzil fragment are different and respectively at dihedral angles of 24° and 66° to the tridentate chelate. The Cl(1)-Cu(1)-Cl(1A) angle, 92.9°, is much shorter than ideal 120° for a tbp geometry. The C(13)-O(1) length, 1.267(2) Å, is consistent to the C=O double bond. The negative charge of the ligand is primarily localized on the [N(2)-N(3)=C(6) ” N(2)=N(3)-C(6)] fragment having comparatively shorter N(2)-N(3) 1.306(2) Å (longer than -N=N- length) and longer N(3)-C(6) 1.335(2) Å (shorter than a N-C length) distances. The C(13)-C(6) length, 1.442(2) Å, is comparable to a C_{sp^2}−C_{sp^2} single bond length. The non-bonding Cu(1)--Cu(1A) distance is 3.348 Å. The Cu(1)-Cl(1), Cu(1)-N(3) and Cu(1)-N(1) distances in **1** are relatively shorter than those reported in similar type of Cu(II) complexes [25].

3.3. Magnetic susceptibility and the EPR spectroscopy

The temperature dependence of the magnetic susceptibility of **1** was studied at 3-300 K using a SQUID magnetometer (1 T external field). A temperature independent effective magnetic moment of 2.58 μ_B was observed above 30 K (Fig. 3). The data were modelled using the isotropic exchange Hamiltonian, $\$_{ex} = -2J\mathbf{S}_1\cdot\mathbf{S}_2$, where J is the isotropic exchange coupling constant and $S_1 = S_2 = {}^1/_2$ for

each Cu(II) d^9 ion. The best fit was obtained with a minute exchange coupling of J = -1.0(1) cm^{-1} (for g = 2.112) in **1** indicates the Cu(II) ions are very weakly coupled by virtue of their co-planarity. This very small exchange coupling precludes assignment of the total spin ground state in **1**, and therefore, J should be treated as an absolute value. The near degenerate singlet-triplet ground state in **1** makes it amenable to interrogation by EPR spectroscopy.

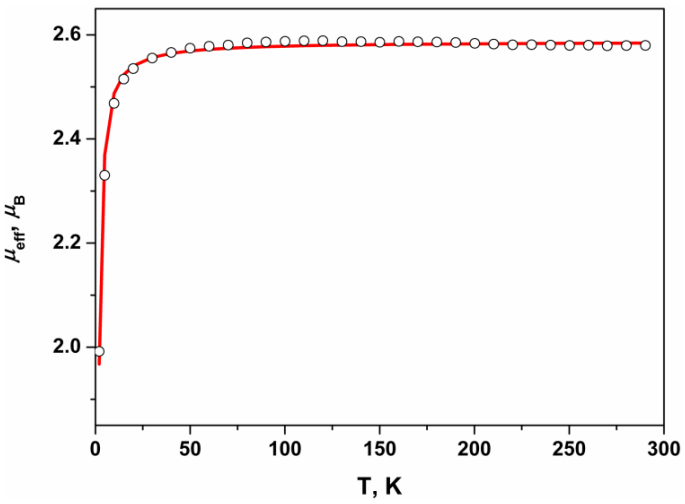

Fig. 3 Temperature dependence of the magnetic moment, μ_{eff}/μ_B, of powdered sample of **1**. The circles represent the experimental data, whereas the solid lines represent simulations (see text).

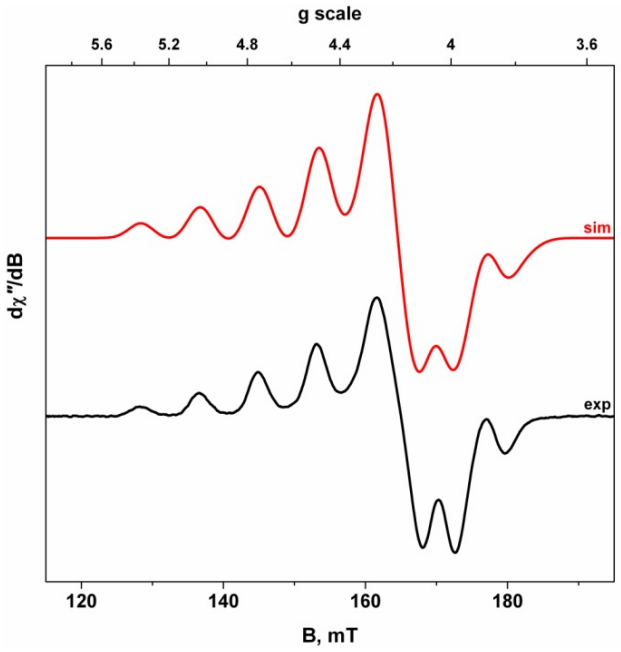

Fig. 4 X-band EPR spectrum of **1** at half-field recorded in CH_2Cl_2/toluene at 10 K. Experimental spectrum shown in black, simulation depicted in red (conditions: frequency 9.632 GHz; power 20 mW; modulation 0.7 mT).

The EPR signal of the allowed transitions (" M_s = 1) was significantly broadened, however we observe a rather striking seven-line feature at half-field (160 mT) signal due to the forbidden •" M_s = 2" transition of the triplet state generated by the weakly coupled Cu(II) ions in **1**. Experimental and simulated X-band EPR spectra were depicted in Fig. 4. The seminal work of Pilbrow and coworkers established the guidelines for interpreting such half-field signals [26] and we simulated the spectrum using *g*, *A*, *J*, and the inter-atomic Cu···Cu distance, *r* = 3.35 Å as determined by X-ray crystallography (*vide supra*). The simulation gave *g* = (2.121, 2.005, 2.004) and *A* = (171, 13, 13) × 10^{-4} cm^{-1} for each Cu(II) ion, The line-shape and overall position was greatly improved by including an Euler angle, ¾= 31°, that is defined as the angle between the inter-atomic Cu···Cu vector and the "z-axis" of the first site, though the exact reference to the coordinate frame was not known. With the extreme broadening of the allowed transitions for **1**, we are unable to unambiguously vet the principle *g* and *A*-values, the mean *g*-value, ⟨*g*⟩ = 2.043 is in good agreement with the one derived from the magnetic data, *g* = 2.112. The *J*-value was fixed from the magnetic susceptibility fit as in this regime with *J* comparable to the microwave energy (0.3 cm^{-1} at X-band), the half-field signal is relatively insensitive to the precise value. On the whole, this spectrum is clearly diagnostic of two weakly coupled Cu(II) d^9 ions with a $d_{x^2-y^2}$ SOMO.

3.4. Electronic structures

The electronic structures of **1** and copper-cuprizone system were elucidated by unrestricted density functional theory (DFT) calculations on **1**, and *cis/trans* isomers of $\mathbf{2^{NO}}$, $\mathbf{2^{NN}}$ and $\mathbf{2^{OO}}$. The gas phase geometry of **1** was optimized by unrestricted DFT calculations respectively with triplet (S = 1) and doublet (S = ½) spin states. Calculated bond parameters summarized in Table 3 are very similar to those observed experimentally in **1**. Structures of two SOMOs of **1** are illustrated in Fig. 5(a). Both the SOMOs are composed of 48% $d_{x^2-y^2}$ (Cu) + 52% ligand. Mulliken spin population analyses have established the following alpha spin distribution in **1**: Cu, 0.50; N1, 0.20; N2, 0.18; O, 0.19. The spin density distribution is illustrated in Fig. 5(b). The calculations therefore conclude that the binding of L^- to the Cu(II) ion results a strong Ã-interaction with the $d_{x^2-y^2}$ orbital and the unpaired electron resides on $Ã^*$ orbital which is composed of $d_{x^2-y^2}$ and a ligand group orbital.

The important outcome of these calculations was that the energies of À$_{imine}$* orbitals of **1** as illustrated in Fig. 6 are higher (alpha À* orbital ~362 kJ/mole and beta orbital ~48 kJ/mole) than the corresponding Ã-antibonding orbitals those are composed of $d_{x^2-y^2}$ and a ligand group orbitals.

(a)

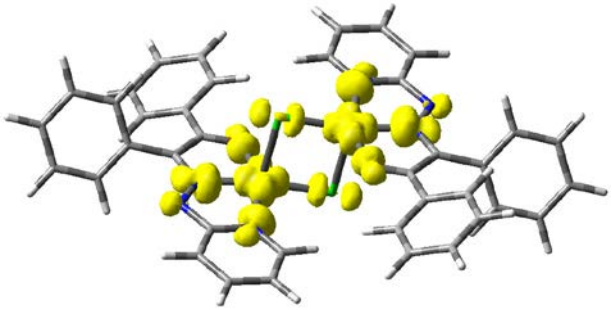

(b)

Fig. 5 (a) Two SOMOs and (b) Mulliken spin density plot of **1**.

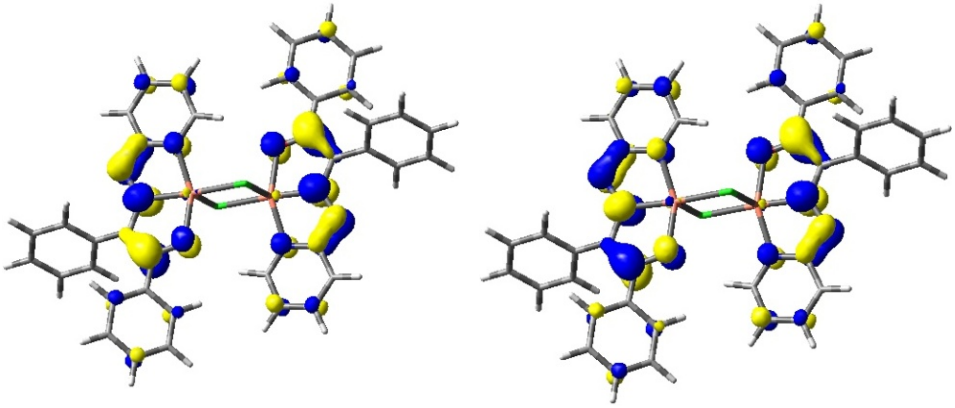

LUMO **LUMO+1**

Fig. 6 Unoccupied alpha À* orbitals of **1**.

In all cases, the SOMO is the Ã-antibonding orbital composed of $d_{x^2-y^2}$ and ligand and likewise the spin density is distributed over the copper ion (~50%) and ligand (~50%). Shifting of spin density to the ligand by this type of interaction makes the Cu(II) to Cu(III) transformation easier, which has enormous effect on structures and reactivities of these species. The experimental observations are: (a) all these species tend to have square-planar geometry, the most favourable geometry of a d^8 ion and (b) these species are reactive and unstable in solutions. All these features can be explained well

by the formation of reactive Cu(III), a d^8 ion which is observed in copper-cuprizone chemistry [8-10].

3.5. Occupied and unoccupied photoactive molecular orbitals (OPMO and UPMOs)

The electronic spectral features of copper cuprizone complex and **1** are very similar. Both species exhibit lower energy absorption bands above 500 nm. The origins of these bands were elucidated by TD DFT calculation on **1**. Sixty lowest singlet excitation energies on the optimized geometries were calculated in dichloromethane using conductor-like polarisable continuum (CPCM) model. Calculated energies, dominant contributions, and transitions types of these calculations were listed in Table 4. The calculated spectrum that correlates well to the experimental spectrum recorded in CH_2Cl_2 is illustrated in Fig. 7. The calculations thus authenticated that the characteristic lower energy absorption is due to the transitions to the unoccupied ² -LUMO, and the ² -SOMO.

Table 4 Excitation energies (»/nm), oscillator strengths (f), transition types and dominant contributions of UV-vis absorption bands of **1** in CH_2Cl_2 obtained from TD DFT calculations.

$»_{cal}$ (nm)	f	$»_{exp}$ (nm)	Significant Transitions (>15%)	Dominant Type
519	0.015	527	² -OCMOs[b] ’ LUMO (90)	L ’ ($d_{x^2-y^2}$ -L)[a]
507	0.388		± HOMO-1 ’ LUMO (22) ± HOMO ’ LUMO (25) ² HOMO-1 ’ LUMO+1(26)	($d_{x^2-y^2}$ +L) ’ L L ’ L L ’ L
482	0.142		± HOMO-1 ’ LUMO (62)	L ’ L
445	0.025		² HOMO-1 ’ LUMO (75)	L ’ ($d_{x^2-y^2}$ -L)[a]
436	0.035		² HOMO-2 ’ LUMO (69)	L ’ ($d_{x^2-y^2}$ -L)[a]
414	0.073		² HOMO-7 ’ LUMO (29) ² HOMO-6 ’ LUMO (30)	(L+d_{z^2}) ’ ($d_{x^2-y^2}$ -L)[a] (L+d_{z^2}) ’ ($d_{x^2-y^2}$ -L)[a]
404.2	0.036		² HOMO-3 ’ LUMO (64)	L ’ ($d_{x^2-y^2}$ -L)[a]
377.8	0.027		² HOMO-9 ’ LUMO (17) ² HOMO-8 ’ LUMO (25)	L ’ ($d_{x^2-y^2}$ -L)[a] L ’ ($d_{x^2-y^2}$ -L)[a]

[a] minus(-) sign designate antibonding orbital
[b]OCMOs = occupied molecular orbitals of ligand

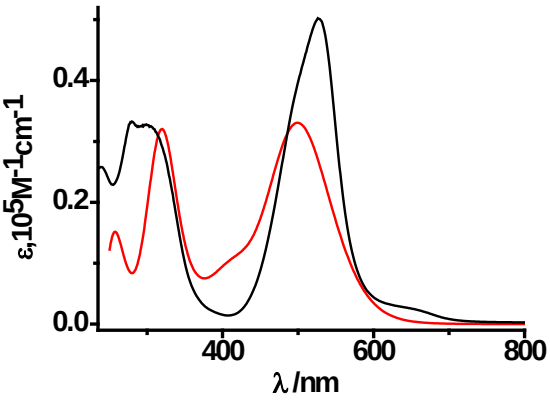

Fig. 7 Experimental (black) and calculated (red) electronic absorption spectra (obtained from TD DFT calculations) of **1** in CH_2Cl_2.

3.6. Electron transfer events (ETEs)

The electron transfer events of **1** in dichloromethane solution under completely N_2 atmosphere were studied by cyclic voltammetry. The experiments predict that all the electron transferred products of **1** are unstable and ETEs are solvent dependent. In dichloromethane solvent, one of the irreversible ETEs that occur at -0.8 V with respect to Fc^+/Fc couple as shown in Fig. 8 are recorded very quickly in different scan rates. The cathodic peak was assigned to the reduction of **1** to $\mathbf{1}^-$ and electron goes to the SOMO that is composed of metal $d_{x^2-y^2}$ and a ligand orbital.

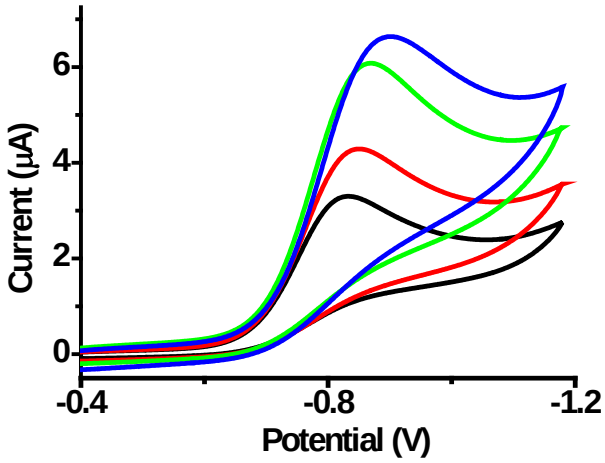

Fig. 8 Cyclic voltammograms of **1** in CH_2Cl_2 at 295 K. Conditions: 0.2 M $[N(n\text{-}Bu)_4]PF_6$ supporting electrolyte; scan rates 50 (black), 100 (red), 200 (green) and 400 (blue) mV s^{-1}; platinum working electrode.

3.7. Molecular and electronic structures of isomeric copper-cuprizone complexes (*cis/trans*-$\mathbf{2}^{\mathbf{NO}}$, $\mathbf{2}^{\mathbf{NN}}$ and $\mathbf{2}^{\mathbf{OO}}$)

In the context of this research, the molecular and electronic structures of copper cuprizone complex were investigated by spin unrestricted DFT calculations. The calculated stable molecular geometry contradicts the existence of reported NN-coordinated copper cuprizone complex. It is unambiguously proved by Messori *et al*. [8] and Nilsson [1] that mono-hydrazone ($L_{mcpz}H_2$, Chart 1) rather than a di-hydrazone actually chelates the Cu(II) ion. The question is whether $L_{mcpz}H_2$ undergoes mono-deprotonation ($L_{mcpz}H^-$) or bis- deprotonation (L_{mcpz}^{2-}), the second process particularly needs removal of a proton from the unfavourable basic -$NHNH_2$ unit. The dominant peak at *m/z* = 457 in the ESI (positive ion) mass spectrum reported by Messori *et al.* [8] is consistent with the presence of only mono-deprotonated ($L_{mcpz}H^-$) mono-hydrazone cuprizone derivative producing neutral $Cu^{II}(L_{mcpz}H)_2$ or cationic $[Cu^{III}(L_{mcpz}H)_2]^+$ products. Chelation of bis-deprotonated (L_{mcpz}^{2-}) cuprizone derivative affords only anionic product, $[Cu^{III}(L_{mcpz}^{2-})_2]^-$ that is detectable in ESI (negative ion) mass spectrum. Further the presence of strong band at 3160 cm^{-1} in FT IR spectrum does not support the presence of bis-deprotonated derivative. To respond all these features of IR and ESI mass spectra, all the possible isomeric geometries (*cis/trans*-$\mathbf{2}^{\mathbf{NN}}$, $\mathbf{2}^{\mathbf{NO}}$ and $\mathbf{2}^{\mathbf{OO}}$; Scheme 1) of the copper cuprizone systems in gas phase were optimized for comparison.

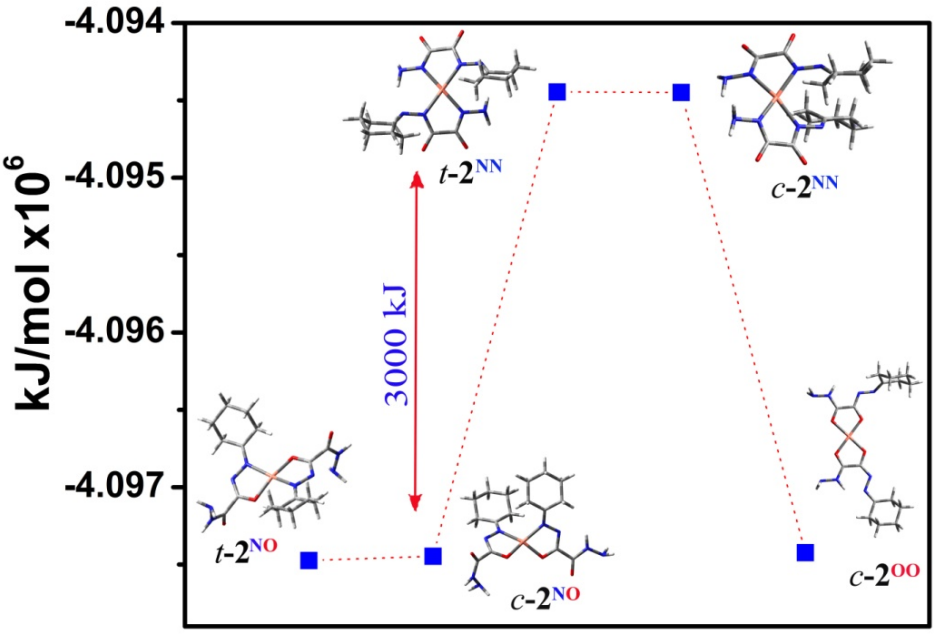

Scheme 2 Relative ground state energies of isomeric copper cuprizone complexes (gas phase).

Surprisingly, it is observed that the ground state energy of ***t*-2^{NN}** (Scheme 1; reported NN-coordinated *trans*-geometry incorporating bis-deprotonated mono-hydrazone cuprizone) or ***c*-2^{NN}** **(**NN-coordinated *cis*-geometry incorporating bis-deprotonated mono-hydrazone cuprizone) is ~3 × 10^3 kJ/mole higher than the most stable alike **1** keto-imine binding, ***t*-2NO** (NO-coordinated *trans*-geometry incorporating mono-deprotonated mono-hydrazone cuprizone like **1**), while the **2^{OO}** (OO-coordinated mono-deprotonated mono-hydrazone cuprizone) is only ~30 kJ/mole higher in energy than ***t*-2NO** or ***c*-2NO** (Scheme 1). A diagram to compare the energies of the isomers is illustrated in Scheme 2. The study forbids the existence of ***t*-2^{NN}** or ***c*-2^{NN}** those were considered so far as the most stable binding mode of cuprizone to copper ion.

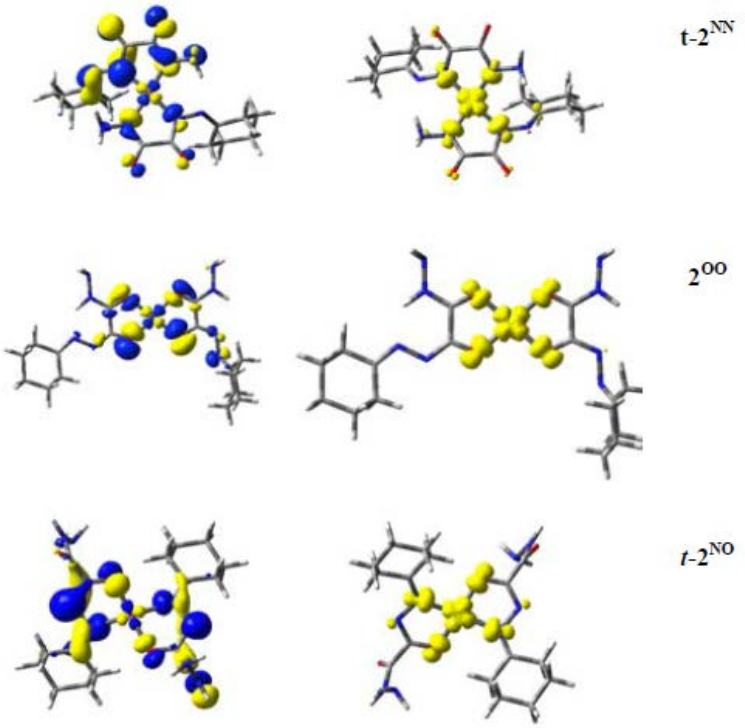

Fig. 9 Structures of SOMOs and Mulliken spin density plots of (a) ***t*-2^{NN}**, (b) ***t*-2NO** and (c) **2^{OO}**.

Analyses of molecular orbitals and atomic spin densities established the electronic structures of ***t*-2^{NN}**, ***c*-2^{NN}**, ***t*-2NO**, ***c*-2NO** and **2^{OO}** complexes. In all cases, similar to **1**, SOMO is an antibonding orbital constituted of d_{Cu} (48-51%) and a ligand group orbital (52-49%) as illustrated in the Fig. 9. The spin density thus is delocalized over the copper (48-51%) as well as on the coordinated N and O donor centers of the ligand (Fig. 9). The feature defines the cuprizone as strong Ã-donor agent. It facilitates the ease removal of the electrons from the cuprizone complexes and augments the

formation of diamagnetic Cu(III)-cuprizone complexes in air [8-10]. The study thus proclaims that coordination of cuprizone to the biologically available copper(II) ion irrespective of the binding mode results stronger reducing equivalent initiating the formation of reactive chemical species like superoxide/peroxide and copper(III) ion which are important sources of the toxic effects of cuprizone to the living systems.

4. Conclusion

An analogue of copper cuprizone complex, $[CuLCl]_2$ (**1**), with (*E*)-1,2-diphenyl-2-(2-(pyridine-2-yl)hydrozono)ethanone (LH), was isolated and substantiated by spectra, single crystal X-ray structure, *SQUID* measurement and unrestricted DFT calculations. The EPR spectroscopy predicts the existence of two weakly coupled Cu(II) d^9 ions in **1**. Electronic structural and spectral features of **1** and copper cuprizone analogues are similar. DFT calculations on all the possible isomeric copper chelates of cuprizone authenticated that mono-deprotonated NO-chelates of mono-hydrazone cuprizone derivative alike **1** affording $Cu(L_{mcpz}H)_2$, (*cis* or *trans*-$\mathbf{2^{NO}}$**)** have the minimum ground state energy, while the *bis*-deprotonated NN-chelates, $[Cu(L_{mcpz})_2]^{2-}$, (*cis* or *trans*-$\mathbf{2^{NN}}$), are ~3×10^3 kJ/mole higher in energy than the corresponding NO-chelates. This result contradicts the formation or existence of so far reported NN-chelated copper cuprizone complex. Molecular orbital analyses revealed that the mixing of $d_{x^2-y^2}$ orbital with a ligand group ÃorbitalofÃ**1** and copper cuprizone shifts 48-50% spin density to the corresponding ligand backbone that make these species reducing agent in the living system.

Acknowledgments

Financial support received from DST (SR/S1/IC/0026/2012) and CSIR (01/2699/12/EMR-II), New Delhi, India is gratefully acknowledged. SK is thankful to CSIR, New Delhi, India, for SRF fellowships.

Appendix A. Supplementary material

X-ray crystallographic CIF file for **1** (CCDC 840632).

References

[1] (a) G. Nilsson, Fresenius'Z. Anal. Chem. 153 (1956) 161; (b) G. Nilsson, Acta Chem. Scand. 4 (1950) 250.

[2] P. Zatta, M. Raso, P. Zambenedetti, W. Wittkowski, L. Messori, F. Piccioli, P. L. Mauri, M. Beltramini, Cell. Mol. Life Sci. 62 (2005) 1502.

[3] (a) G. R. Clark, B. W. Skelton, T. N. Waters, J. Chem. Soc. Dalton Trans. (1976) 1528; (b) G. R. Clark, B. W. Skelton, T. N. Waters, J. Chem. Soc. Chem. Commun. (1972) 1163.

[4] J. Oliver, T. N. Waters, J. Chem. Soc. Chem. Commun. (1982) 1111.

[5] W. E. Keyes, J. B. R. Dunn, T. M. Loehr, J. Am. Chem. Soc. 99 (1977**)** 4527.

[6] (a) I. O. Fritsky, H. Kozlowski, O. M. Kanderal, M. Haukka, J. S.-Kozlowska, E. G.-Kontecka, F. Meyer, Chem. Commun. (2006) 4125; (b) I. O. Fritsky, H. Kozlowski, P. J. Sadler, O. P. Yefetova, J. S.-Kozlowska, V. A. Kalibabchuk, T. Glowiak, J. Chem. Soc. Dalton Trans. (1998) 3269.

[7] (a) I. H. Pattison, J. N. Jebbett, Res. Vet. Sci.14 (1973) 128; (b) I. H. Pattison, J. N. Jebbett, J. Pathol. 109 (1973) 245; (c) I. H. Pattison, J. N. Jebbett, Nature 230 (1971) 115; (d) I. H. Pattison, J. N. Jebbett, Res. Vet. Sci.12 (1971) 378.

[8] L. Messori, A. Casini, C. Gabbiani, L. Sorace, M. M.-Miranda, P. Zatta, Dalton Trans. (2007) 2112.

[9] M. M.-Miranda, M. Pagliai, G. Cardini, L. Messori, B. Bruni, A. Casini, M. Di Vaira, V. Schettino, Cryst. Eng. Comm. 10 (2008) 416.

[10] N. Yamamoto, K. Kuwata, J. Mol. Str. 52 (2009) 52.

[11] (a) S. C. Patra, M. K. Biswas, A. N. Maity, P. Ghosh, Inorg. Chem. 50 (2011) 1331; (b) A. S. Roy, H. M. Tuononen, S. P. Rath, P. Ghosh, Inorg. Chem.46 (2007) 5942.

[12] G. R. Hanson, K. E. Gates, C. J. Noble, M. Griffin, A. Mitchel, S. Benson, J. Inorg. Biochem. 98 (2004) 903.

[13] (a) G. M. Sheldrick, *ShelXS97*; Universität Göttingen: Göttingen, Germany, 1997; (b) G. M. Sheldrick, *ShelXL97*; Universität Göttingen: Göttingen, Germany, 1997.

[14] M. J. Frisch, G. W. Trucks, H. B. Schlegel, G. E. Scuseria, M. A. Robb, J. R. Cheeseman, Jr. J. A. Montgomery, T. Vreven, K. N. Kudin, J. C. Burant, J. M. Millam, S. S. Iyengar, J. Tomasi, V. Barone, B. Mennucci, M. Cossi, G. Scalmani, N. Rega, G. A. Petersson, H. Nakatsuji, M. Hada, M. Ehara, K. Toyota, R. Fukuda, J. Hasegawa, M. Ishida, T. Nakajima, Y. Honda, O. Kitao, H. Nakai, M. Klene, X. Li, J. E. Knox, H. P. Hratchian, J. B. Cross, V. Bakken, C. Adamo, J. Jaramillo, R. Gomperts, R. E. Stratmann, O. Yazyev, J. A. Austin, R. Cammi, C. Pomelli, J. W. Ochterski, P. Y. Ayala, K. Morokuma, G. A. Voth, P. Salvador, J. J. Dannenberg, V. G. Zakrzewski, S. Dapprich, A. D. Daniels, M. C. Strain, O. Farkas, D. K. Malick, A. D. Rabuck, K. Raghavachari, J. B. Foresman, J. V. Ortiz, Q. Cui, A. G. Baboul, S. Clifford, J. Cioslowski, B. B. Stefanov, G. Liu, A. Liashenko, P. Piskorz, I. Komaromi, R. L. Martin, D. J. Fox, T. Keith, M. A. Al-Laham, C. Y. Peng, A. Nanayakkara, M. Challacombe, P. M. W. Gill, B. Johnson, W. Chen, M. W. Wong, C. Gonzalez, J. A. Pople, *Gaussian 03, revision E.01*; Gaussian, Inc.: Wallingford, CT, 2004.

[15] (a) R. G. Parr, W. Yang, Density Functional Theory of atoms and molecules; Oxford University Press: Oxford, UK, 1989; (b) D. R. Salahub, M. C. Zerner, The Challenge of d and f Electrons; ACS Symposium Series 394; American Chemical Society: Washington, DC, 1989; (c) W. Kohn, L. Sham, J. Phys. Rev. 104 (1965) A1133; (d) P. Hohenberg, W. Kohn, Phys. Rev. 136 (1964) B864.

[16] (a) R. E. Stratmann, G. E. Scuseria, M. Frisch, J. Chem. Phys. 109 (1998) 8218; (b) M. E. Casida, C. Jamoroski, K. C. Casida, D. R. Salahub, J. Chem. Phys. 108 (1998) 4439; (c) R. Bauernschmitt, M. Haser, O. Treutler, R. Ahlrichs, Chem. Phys. Lett. 256 (1996) 454.

[17] (a) A. D. Becke, J. Chem. Phys. 98 (1993) 5648; (b) B. Miehlich, A. Savin, H. Stoll, H. Preuss, Chem. Phys. Lett. 157 (1989) 200; (c) C. Lee, W. Yang, R. G. Parr, Phys. Rev. B 37 (1988) 785.

[18] P. J. Pulay, Comput. Chem. 3 (1982) 556.

[19] H. B. Schlegel, J. J. McDouall, In Computational Advances in Organic Chemistry; C. Ogretir, I. G. Csizmadia, Eds.; Kluwer Academic: The Netherlands, 1991; pp 167-185.

[20] (a) P. J. Hay, W. R. Wadt, J. Chem. Phys. 82 (1985) 270; (b) W. R. Wadt, P. J. Hay, J. Chem. Phys. 82 (1985) 284; (c) P. J. Hay, W. R. Wadt, J. Chem. Phys. 82 (1985) 299.

[21] (a) V. A. Rassolov, M. A. Ratner, J. A. Pople, P. C. Redfern, L. A. Curtiss, J. Comput. Chem. 22 (2001) 976; (b) M. M. Francl, W. J. Pietro, W. J. Hehre, J. S. Binkley, D. J. DeFrees, J. A. Pople, M. S. Gordon, J. Chem. Phys. 77 (1982) 3654; (c) P. C. Hariharan, J. A. Pople, Mol. Phys. 27 (1974) 209; (d) P. C. Hariharan, J. A. Pople, Theo. Chim. Acta. 28 (1973) 213; (e) W. J. Hehre, R. Ditchfield, J. A. Pople, J. Chem. Phy. 56 (1972) 2257.

[22] (a) G. A. Petersson, M. A. Al-Laham, J. Chem. Phys. 94 (1991) 6081; (b) G. A. Petersson, A. Bennett, T. G. Tensfeldt, M. A. Al-Laham, W. A. Shirley, J. Mantzaris, J. Chem. Phys. 89 (1988) 2193.

[23] N. M. O'Boyle, A. L. Tenderholt, K. M. Langner, J. Comput. Chem. 29 (2008) 839.

[24] (a) M. Cossi, N. Rega, G. Scalmani, V. Barone, J. Comput. Chem. 24 (2003) 669; (b) V. Barone, M. Cossi, J. Phys. Chem. A 102 (1998) 1995.

[25] (a) S. Delgado, A. Gallego, O. Castillob, F. Zamora, Dalton Trans. 40 (2011) 847; (b) M. Du, Y. M. Guo, X. H. Bu, J. Ribas, M. Monfort, New J. Chem. 26 (2002) 939; (c) M. M. Kimani, D. VanDerveer, J. L. Brumaghim, Acta Cryst. C67 (2011) m208; (d) A. N. Papadopoulos, V. Tangoulis, C. P. Raptopoulou, A. Terzis, D. P. Kessissoglou, Inorg. Chem. 35 (1996) 559.

[26] (a) A. Skorobogaty, T. D. Smith, G. Dougherty, J. R. Pilbrow, J. Chem. Soc., Dalton Trans. (1985) 651; (b) A. D. Toy, M. D. Hobday, P. D. W. Boyd, T. D. Smith, J. R.

Pilbrow, J. Chem. Soc., Dalton Trans. (1973) 1259; (c) A. D. Toy, T. D. Smith, J. R. Pilbrow, J. Chem. Soc., Dalton Trans. (1973) 2498; (d) P. D. W. Boyd, A. D. Toy, T. D. Smith, J. R. Pilbrow, J. Chem. Soc., Dalton Trans. (1973) 1549; (e) J. H. Price, J. R. Pilbrow, K. S. Murray, T. D. Smith, J. Chem. Soc. A (1970) 968; (f) P. D. W. Boyd, J. R. Pilbrow, T. D. Smith, Aust. J. Chem. 24 (1971) 59.

Graphical contents entry

Molecular and electronic structures of $[CuLCl]_2$ (**1**), (LH = (*E*)-1,2-diphenyl-2-(2-(pyridine-2-yl) hydrozono)ethanone) were reported and compared with that of isomeric copper cuprizone complex (*cis/trans*-$\mathbf{2}^{\mathbf{NO}}$, $\mathbf{2}^{\mathbf{NN}}$, $\mathbf{2}^{\mathbf{OO}}$).